Electronic Supplementary Material (ESI) for Nanoscale.

Supporting information for: Plasmonic isomers formed via DNA-based self-assembly of gold nanoparticles

Laurent Lermusiaux* and Alison M. Funston*

ARC Centre of Excellence in Exciton Science and School of Chemistry, Monash University, Clayton, VIC, 3800

E-mail: laurent.lermusiaux@monash.edu; alison.funston@monash.edu

*To whom correspondence should be addressed

Tetrahedral DNA templates

a Symmetrical assembly

DNA	Sequences - 5′ to 3′
1	trithiol-TTTT CTCACTAAGATCGATAGAGCGATTGTGATA TTT CAAGCGGTACTC-CAGCTCTAGGTAGCTCCC TTT CCAATCAGCTTATGTGAGCGCCTGCCCATG
2	trithiol-TTTT GTGCTCAGGATTGCAGCAACAGTGATCGGT TTT CTGCGCTGTATA-GGGACTGTGCTACAGAGA TTT CATGGGCAGGCGCTCACATAAGCTGATTGG
3	trithiol-TTTT ACCGATCACTGTTGCTGCAATCCTGAGCAC TTT GGGAGCTACCTA-GAGCTGGAGTACCGCTTG TTT AGGTTGACCGCAGTGTGAATGACTCAAGGC
4	trithiol-TTTT TATCACAATCGCTCTATCGATCTTAGTGAG TTT TCTCTGTAGCA-CAGTCCCTATACAGCGCAG TTT GCCTTGAGTCATTCACACTGCGGTCAACCT

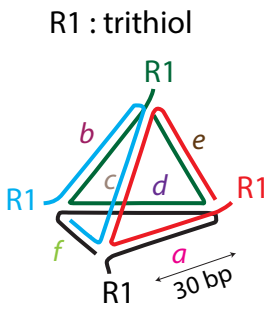

b Asymmetrical assembly

DNA	Sequences - 5′ to 3′
5	thiol-TTT CTCACTAAGAGCGATAGAGCGATTGTGATA TTT TCCAATCAGCTTATG TGAGCGCCTGCCCAT TTT GAAGCGGTACTCCAGCTCTAGGTAGCTCCC
6	thiol-TTT TATCACAATCGCTCTATCGCTCTTAGTGAG TTT CCTTGAGTCATTCA-CACTGCGGTCAACCTG TTT TCTCTGTAGCACAGTCCCTATACAGCGCAT
7	thiol-TTT CAGGTTGACCGCAGTGTGAATGACTCAAGG TTT GGGAGCTACCTA GAGCTGGAGTACCGCTTC TTT CCGATCACTGTTGCTGCAATCCTGAGCACA
8	thiol-TTT ATGGGCAGGCGCTCACATAAGCTGATTGGA TTT ATGCGCTGTATAGGG ACTGTGCTACAGAGA TTT TGTGCTCAGGATTGCAGCAACAGTGATCGG

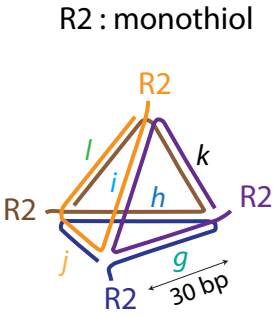

c Interparticle distance estimation

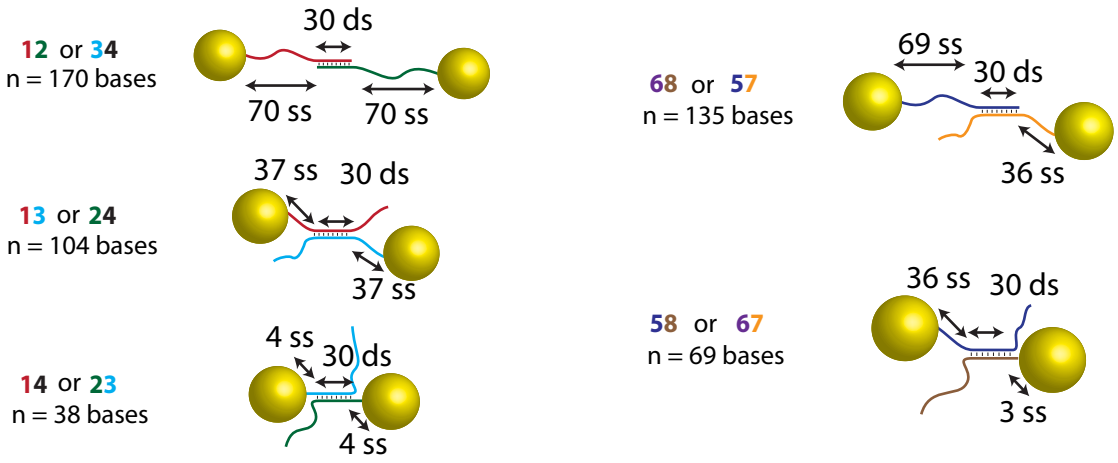

Figure S1: Tetrahedral DNA template sequences. (a-b) DNA sequences for the (a) symmetrical and (b) asymmetrical assembly scheme and corresponding tetrahedral DNA. Complementary strands are denoted by the same colour. (c) Estimation of the dimer interparticle distance using the number of DNA bases.

Table S1: Summary of the different experimental conditions - gold nanoparticle passivation ligand, salt concentration and temperature - used during the tetramer synthesis using different hybridisation pathways. The figures showing the associated purification electrophoresis gels are listed in the last column. Asterisks in the Pathway column denote optimised electrophoresis gels. When a thermal treatment was used, samples were placed at the indicated temperature with either a slow decrease overnight or a rapid cooling after five minutes mentioned as 'anneal'.

Pathway	Surface chemistry	[NaCl] (mM)	[$MgCl_2$] (mM)	Temperature (°C)	Figure
P1 to **P8**	PEG	150	0	RT	1b, S6
***P1** to **P3**	BSPP	80	0	RT	3a
***P3**	PEG	150	0	RT	3c, S7d
P1 to **P3**	PEG	300	0	40	3d
P2	PEG	50	0	90	3f
P2	PEG / BSPP	150 / 80	0	RT	S5a
P4	BSPP	80	0	RT	S7a
P4	BSPP	0/50/50	1.25/1.25/0	95 (anneal)	S7a
P4	PEG	100	7.5	RT/95 (anneal)	S7a
P2	PEG	80	0	RT/37	S7b
P2	PEG	150	0	RT/37	S7b
***P1**	BSPP	80	0	RT/65	S7c
***P1**	PEG	300	0	RT/65	S7c
***P4**	PEG	300	0	65	S7c
***P3**	BSPP	60	0	RT	S7d

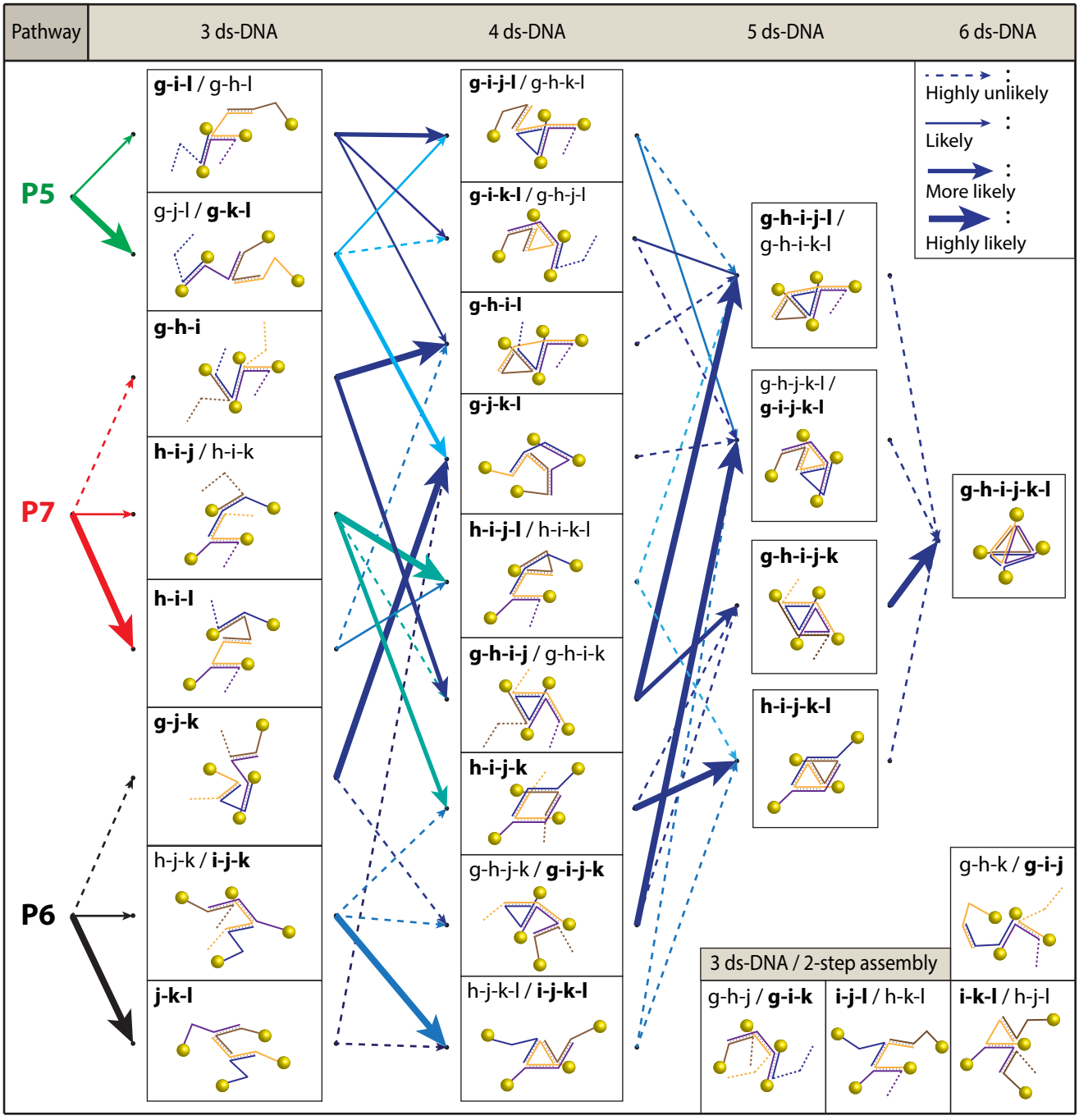

Figure S2: Hybridisation pathway tree of the asymmetrical assembly. Schematic representation of the 26 possible structural isomers. Single-stranded DNA sub-sequences are represented by a dotted line when one of end is free. The naming system indicates all the ds-strand of the isomer (letters correspond to specific ds sub-sequences described in Figure 1a and Supplementary Fig. S1a). The name in bold indicates the tetramer schematised in the box. Green, black and red arrows point to isomers firstly synthesised by pathway **P5** to **P7** respectively. Blue arrows represent possible intra-structure hybridisation. Dotted arrows represent unlikely event, increasingly thicker arrows indicate increased likelihood of the hybridisation step to occur.

The hybridisation tree of the asymmetrical assembly shows more possibilities of intra-hybridisation schemes than the symmetrical one. These intra-hybridisations can involve:

- two strands with free ends. They are denoted by a thick arrow ('highly likely'). If a single isomer can hybridise through two different pathways and each involves two strands with free ends, the pathway involving sub-sequences closer to the gold nanoparticles is represented with a intermediate sized arrow (denoted as 'more likely' in the legend).

- one strand with a free end. In this case, they are denoted by a thin arrow as the event is possible, but probably slow, because it requires the structure to distort in order to form the double strand. If a single isomer can hybridise through two different pathways and each involves one strand with a free end, the pathway involving sub-sequences further away to the gold nanoparticles is denoted by an intermediate sized arrow (denoted as 'more likely' in the legend).

- no strand with a free end. In this case, they are all denoted by dotted arrows as they are highly unlikely.

Complementary electrophoresis

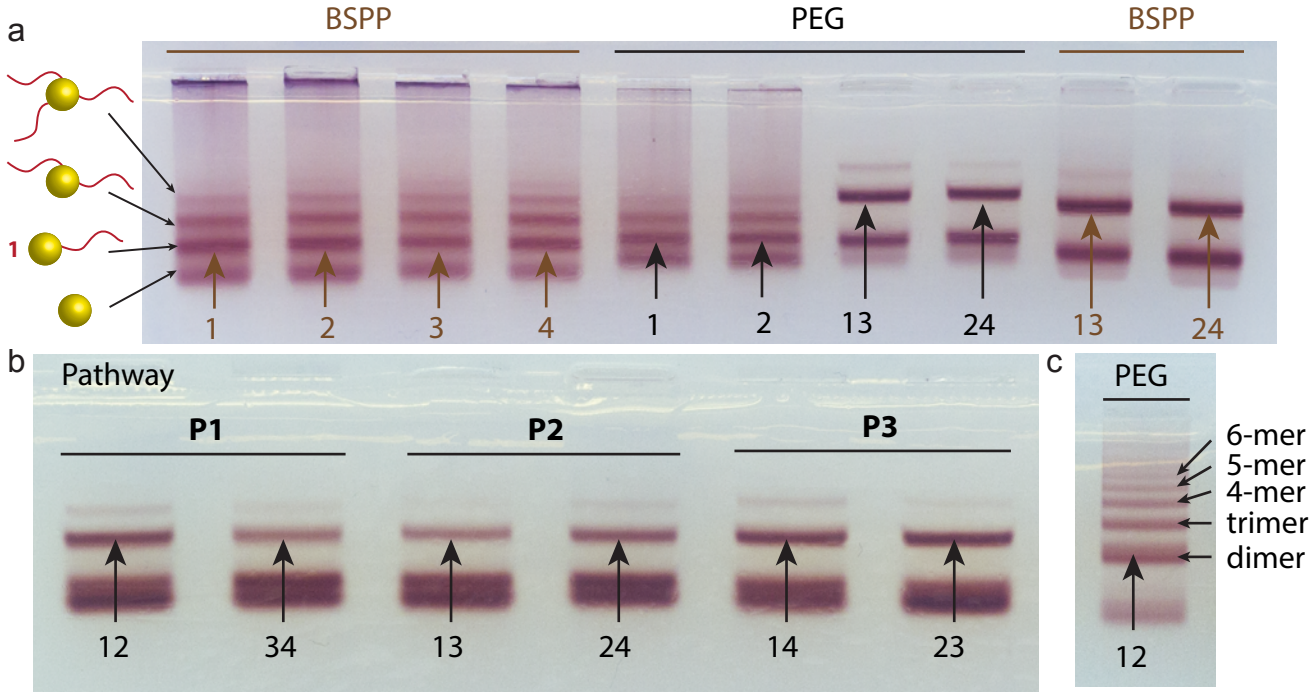

Figure S3: Complementary electrophoresis purification of monoconjugated spheres and dimers. (a) Purification of monoconjugated structures **1**, **2**, **3** and **4** and dimers **13** and **24**, with BSPP or PEG-passivated gold nanoparticle. (b) Purification of dimers for pathways **P1** to **P3**. (c) Purification of dimer **12** when the numbers of DNA strands is not controlled on the gold nanoparticle surface.

Supplementary Figure S3a shows the electrophoretic purification of nanoparticles conjugated with a single 100-base long DNA tethered on their surface from unconjugated (lowest band) and poly-conjugated (upper bands) gold nanoparticles. The clear separation of the different bands demonstrates that we can reliably extract monoconjugated spheres to avoid any undesired structures in the following steps of the tetramer synthesis. Supplementary Figure S3c shows the numerous by-products (multiple bands corresponding to structures with more than two nanoparticles) of a dimer synthesis performed with poly-conjugated gold nanoparticles. This demonstrates the importance of controlling the number of DNA strands attached to gold nanoparticles.

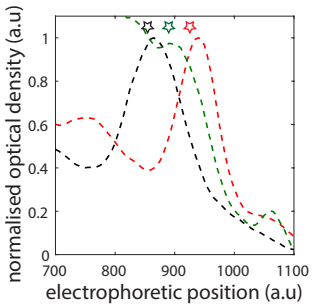

Figure S4: Cross-sections of Figure 1b. Normalised cross-sections of the tetramer band along the migration axis for pathways **5** (green dotted line), **6** (black dotted line) and **7** (red dotted line)

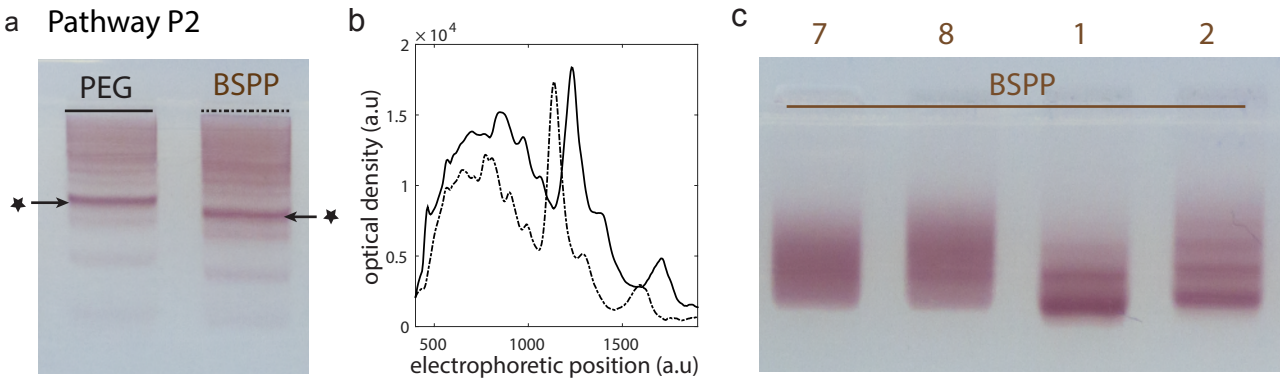

Figure S5: Effect of the PEG passivation on the self-assembly. (a-b) Electrophoresis purification (a) and corresponding cross-sections (b) of tetramers synthesised using pathway **P2** prepared with PEG- (left column, black solid line) or BSPP-passivated (right column, dotted black line) gold nanoparticles. (c) Purification of structures **7**, **8**, **1** and **2** (from left to right) using BSPP-passivated nanoparticles.

Supplementary Figure S5a-b show that the passivating ligand used did not affect the DNA self-assembly as we observe identical products for both ligands when using the same pathway. However, the purification of BSPP-passivated gold nanoparticles with two of the monothiolated DNA strand (Structures **7** and **8** in Supplementary Fig. S5c) did not provide sufficiently distinct bands to confidently isolate monoconjugated gold nanoparticles. Therefore, BSPP-passivated spheres were only used with trithiolated DNA.

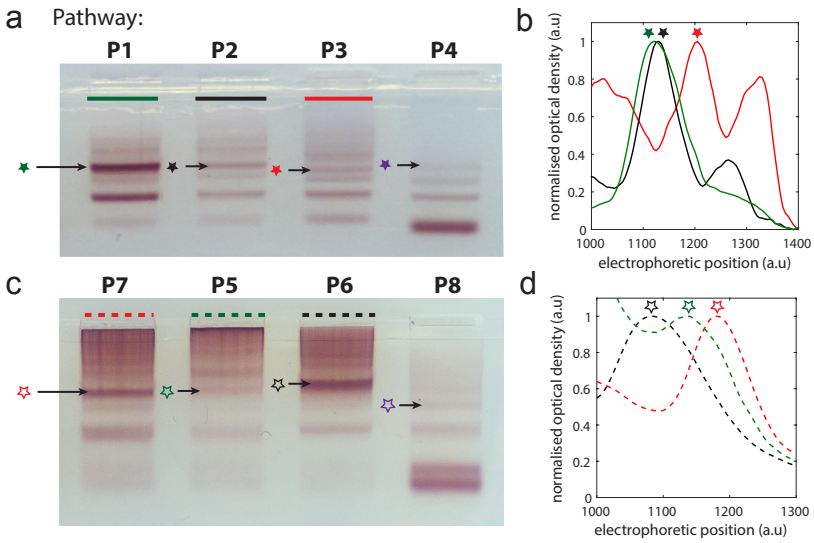

Figure S6: (a-c) Electrophoretic purification of tetramers synthesised through pathways (a) **P1** to **P4** (c) and **P5** to **P8**. Tetramers bands are indicated by arrows and stars. (b-d) Normalised cross-sections of the tetramer band along the migration axis of (b) panel a and (d) panel c.

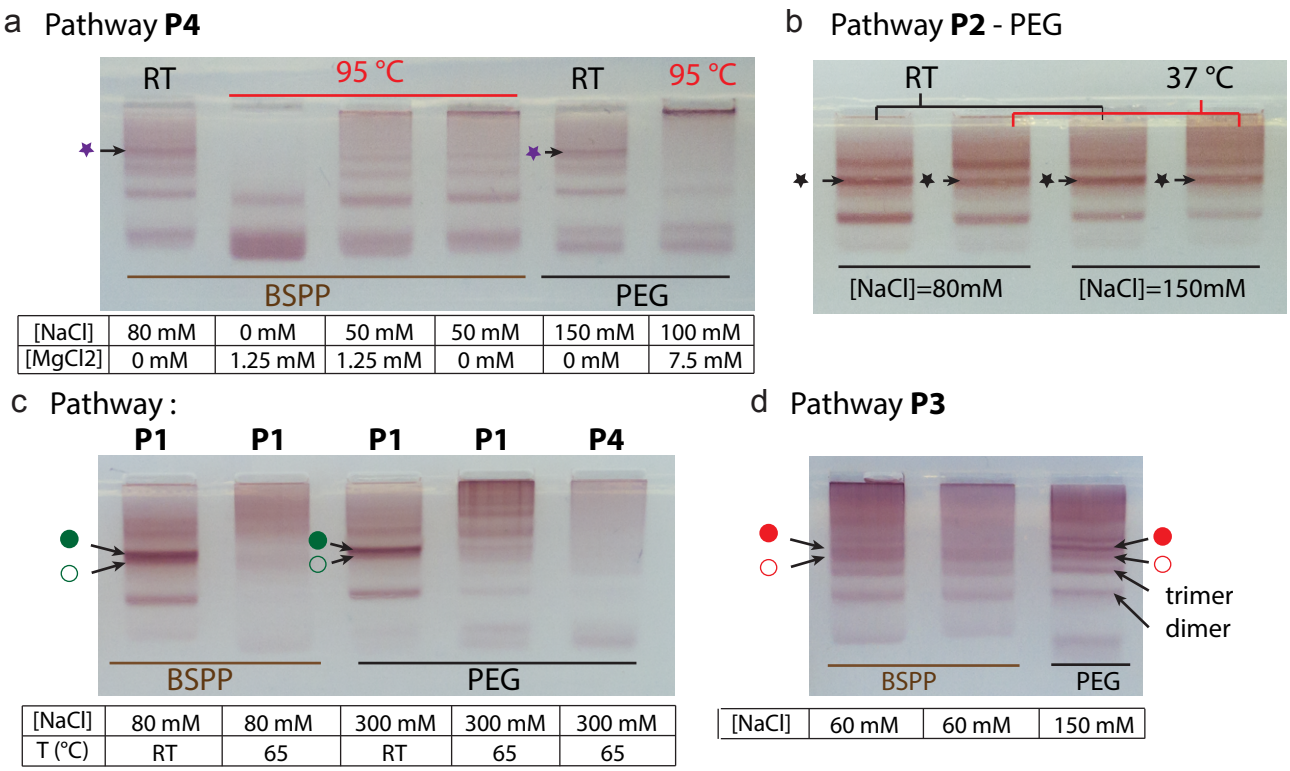

[NaCl]	80 mM	0 mM	50 mM	50 mM	150 mM	100 mM
[MgCl2]	0 mM	1.25 mM	1.25 mM	0 mM	0 mM	7.5 mM

[NaCl]	80 mM	80 mM	300 mM	300 mM	300 mM
T (°C)	RT	65	RT	65	65

[NaCl]	60 mM	60 mM	150 mM

Figure S7: Electrophoretic purification of tetramers synthesised through different pathways and under different experimental conditions. (a) Comparison of products yielded from pathway **P4** at room temperature or with an annealing treatment at 95 °C for 5 minutes and different NaCl and $MgCl_2$ concentrations or surface chemistries as detailed on the image. (b) Comparison of products yielded from pathway **P2** at room temperature or at 37 °C followed by a slow temperature decrease overnight and different NaCl concentrations. (c) Comparison of products yielded from pathways **P1** and **P4** at room temperature or at 65 °C followed by a slow temperature decrease overnight and different NaCl concentrations and surface chemistries. (d) Electrophoretic purification of tetramers yielded from pathway **P3** at room temperature with BSPP- and PEG-passivated gold nanoparticles.

Table S2: Dimer interparticle distance (in number of DNA bases) and PEG-passivated gold nanoparticle tetramer yields calculated from TEM images showing on average 10 tetramers per frame for a total of more than 1300 tetramers, for different pathways (see Supplementary Fig. S8 for TEM images). Purified samples were deposited at two different NaCl concentrations (50 or 200 mM).

Pathway	Dimer interparticle distance (number of DNA bases)	Tetramer yield (@ 50 mM)	Tetramer yield (@ 200mM)
P1	170	50 % (64/127)	85 % (118/139)
P2	104	67 % (144/215)	75 % (155/208)
P3	38	53 % (196/369)	74 % (70/94)
P4	NA	NA	51 % (134/261)
P5	g: 68 - l: 168	75 % (84/112)	NA
P6	135	61 % (245/399)	NA
P7	69	45 % (123/276)	NA

Additional EM images

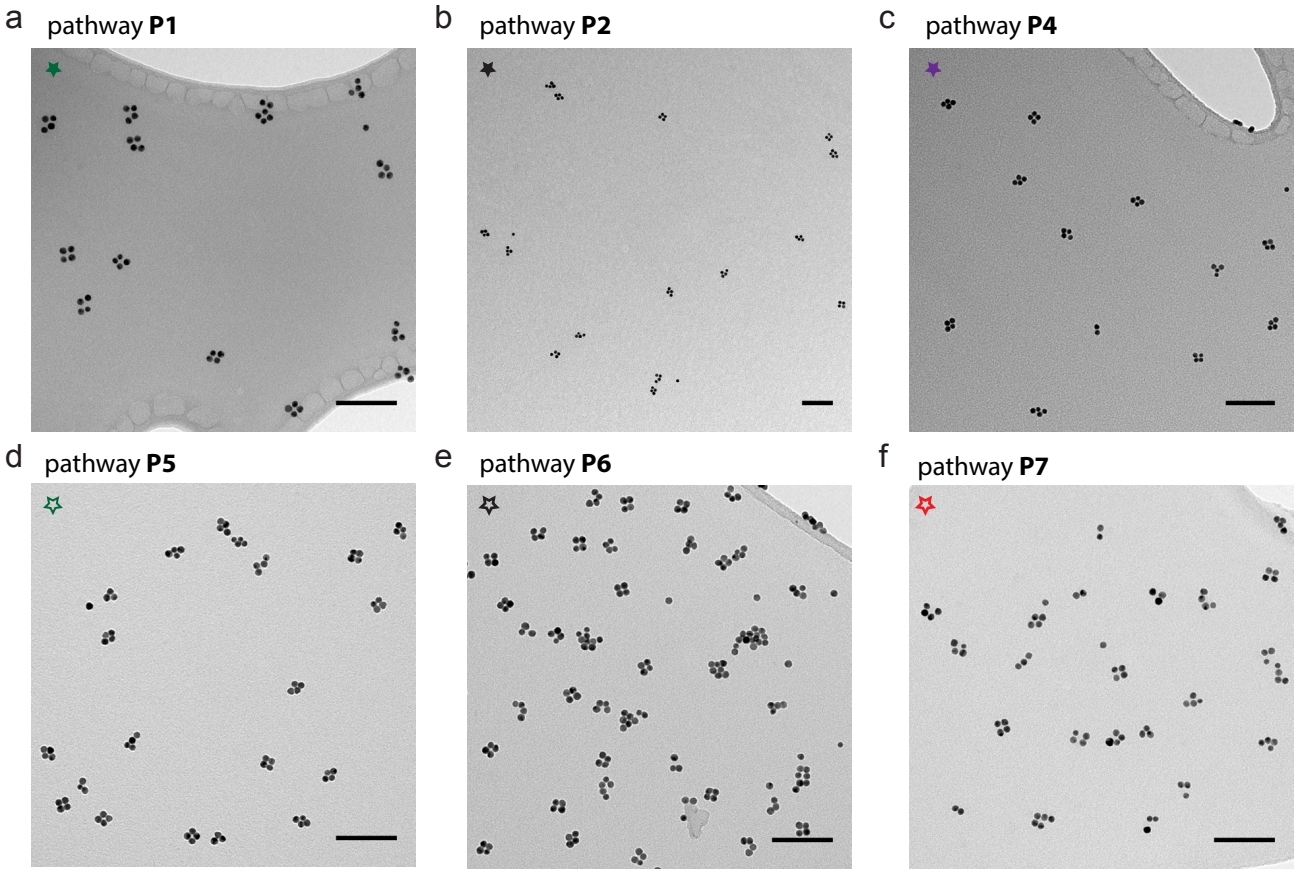

Figure S8: (a-f) TEM images of purified tetramers synthesised using pathways **P1** (a), **P2** (b), **P4** (c), **P5** (d), **P6** (e) and **P7** (f). Scale bars are 100 nm. Stars indicate the corresponding tetramer bands in Figure 1b.

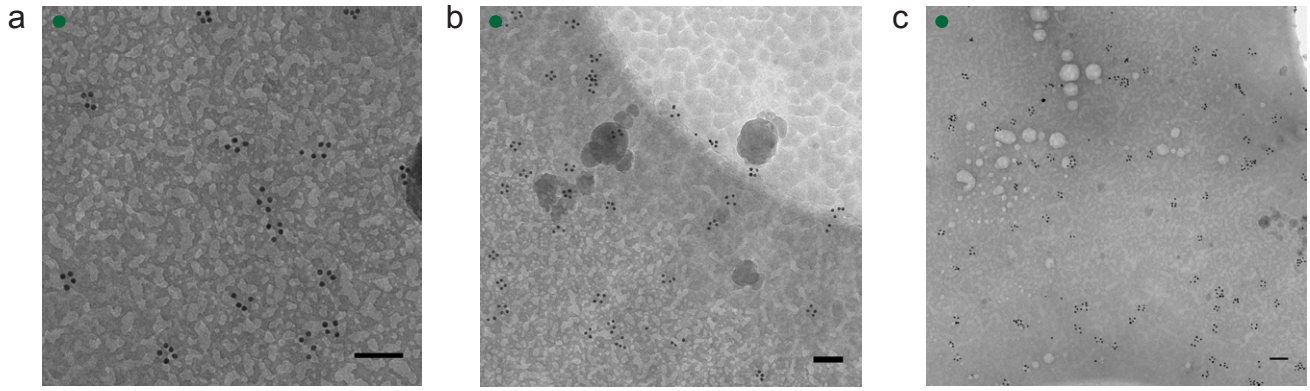

Figure S9: (a-c) Complementary widefield Cryo-TEM images of the isomer 2-3-3. Scale bars are 100 nm. Circles indicate the corresponding isomer structure in Figure 2d.

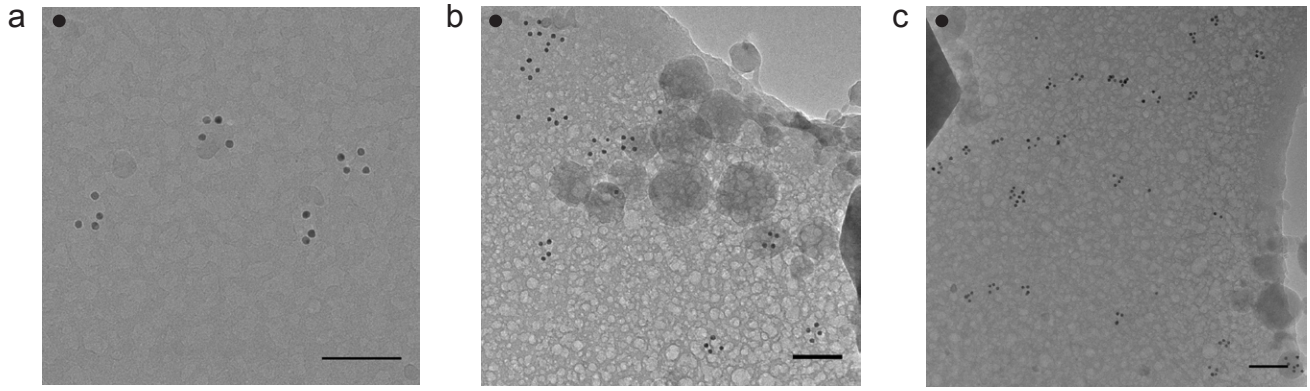

Figure S10: (a-c) Complementary widefield Cryo-TEM images of the isomer 2-2-3-3. Scale bars are 100 nm. Circles indicate the corresponding isomer structure in Figure 2d.

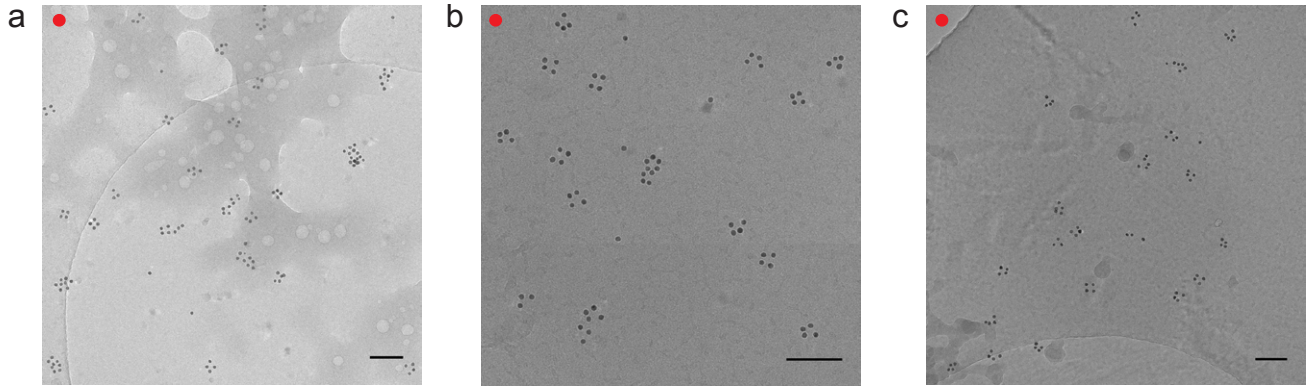

Figure S11: (a-c) Complementary widefield Cryo-TEM images of the isomer 1-1-3-3. Scale bars are 100 nm. Circles indicate the corresponding isomer structure in Figure 2d.

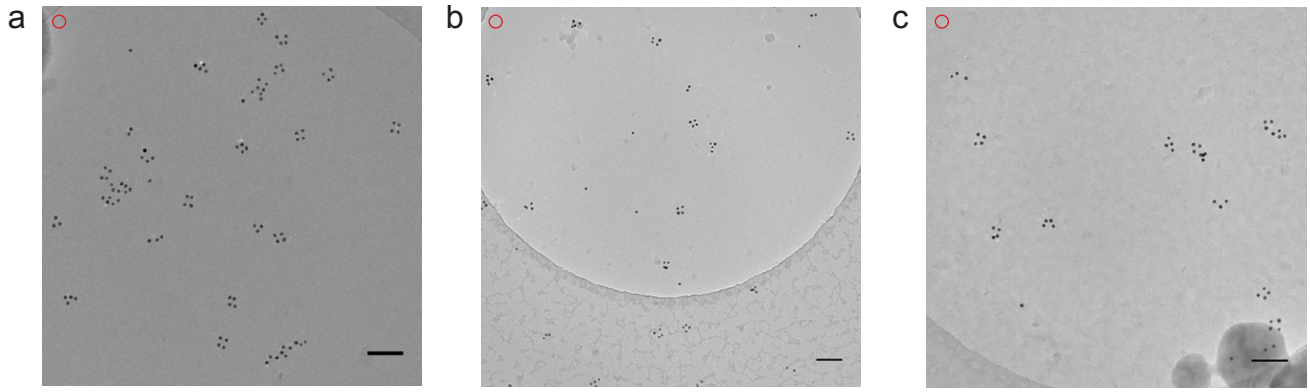

Figure S12: (a-c) Complementary widefield Cryo-TEM images of the isomer 1-1-2-3-3. Scale bars are 100 nm. Circles indicate the corresponding isomer structure in Figure 2d.

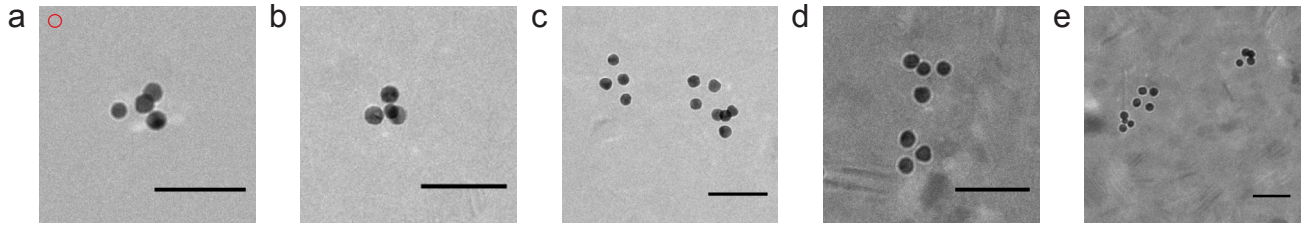

Figure S13: (a-e) Close-up Cryo-TEM images of the isomer 1-1-2-3-3 exhibiting three-dimensional features. Scale bars are 50 nm. The circle indicates the corresponding isomer structure in Figure 2d.

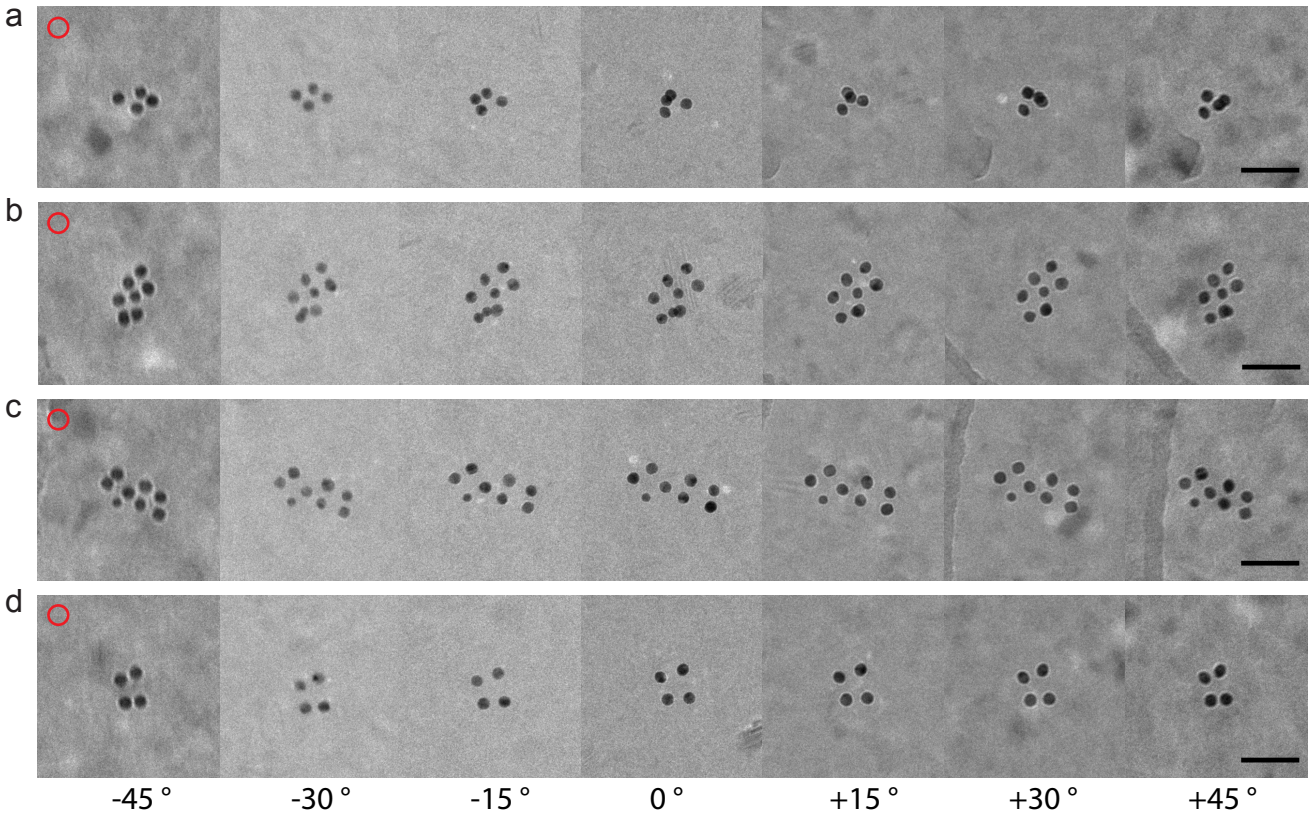

Figure S14: (a-d) Close-up Cryo-TEM image series of the isomer 1-1-2-3-3 tilted at different angles, from left to right : -45 °, -30 °, -15 °, 0 °, +15 °, +30 ° and +45 °. Scale bars are 50 nm. Circles indicate the corresponding isomer structure in Figure 2d.

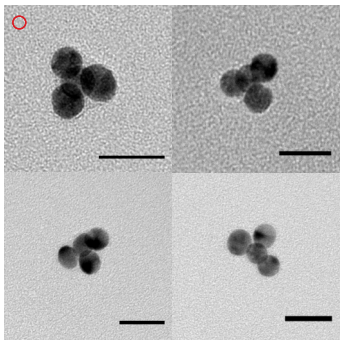

Figure S15: (a) Close-up TEM images of 4 deposited gold nanoparticle tetrahedra. Scale bars are 20 nm. Circles indicate the corresponding isomer structure in Figure 2d.

Statistical analysis of Cryo-EM images

Interparticle distance measurements

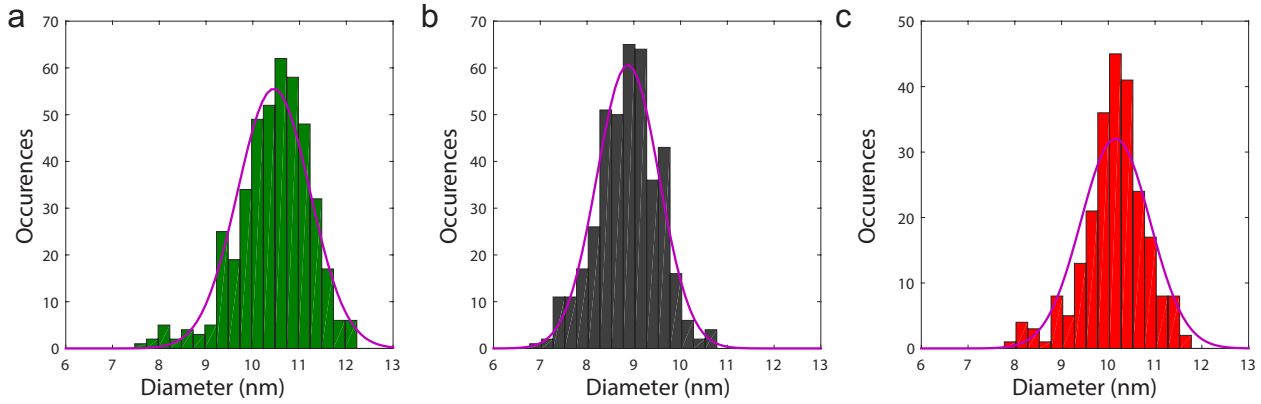

Figure S16: Gold nanoparticle diameter distributions measured on EM images with corresponding Gaussian fits: (a) 10.5 ± 0.8 nm (b) 8.9 ± 0.7 nm (c) and 10.2 ± 0.7 nm. Each histogram corresponds to a different nanoparticle batch. The same nanoparticle batches were used to synthesise tetramers which are analysed in the corresponding histograms in Supplementary Figure S17.

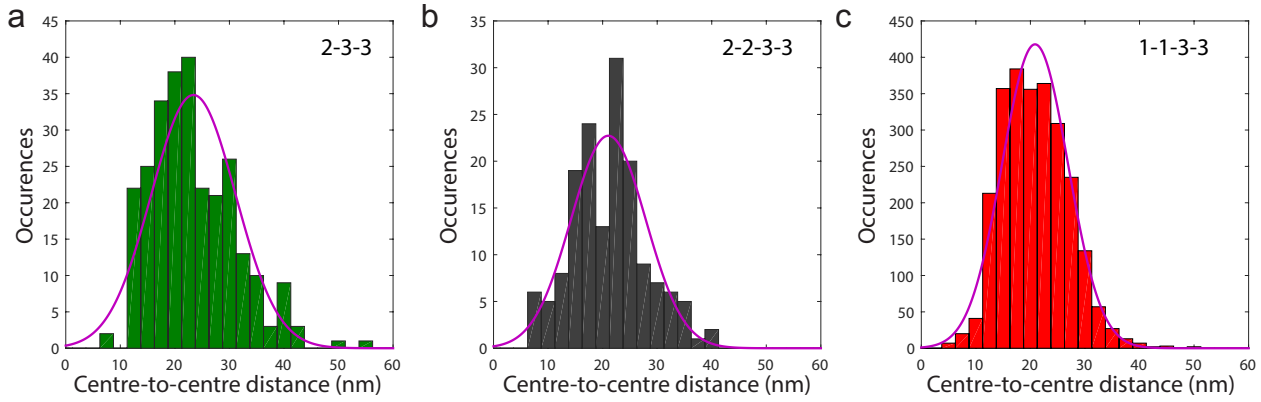

Figure S17: Projected centre-to-centre distance distributions in isomers (a) 2-3-3, (b) 2-2-3-3 and (c) 1-1-3-3, measured on Cryo-EM images and presented with a Gaussian fit (a) 23.4 ± 7.7 nm (b) 21.0 ± 6.8 nm (c) 20.9 ± 6.0 nm.

We can qualitatively compare the hydrodynamic volume of the three different isomers 2-3-3, 2-2-3-3 and 1-1-3-3 using cryo-EM images, by calculating an average projected interparticle distance for each isomer. For each tetramer, we extracted 6 centre-to-centre distances

(noted l_1 to l_6 in Supplementary Fig. S18a) and plotted the corresponding distributions in Supplementary Figure S17. The interparticle distance was obtained by deconvoluting the gold nanoparticle diameter distribution (calculated in Supplementary Fig. S16) from the centre-to-centre distribution and results are presented in the main text.

Theoretical projected tetrahedron

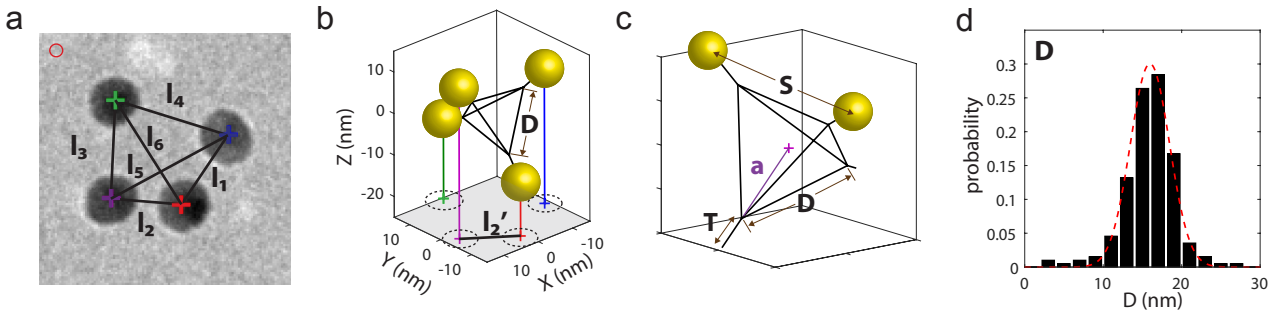

Figure S18: (a-b) Cryo-EM close-up image of an isomer 1-1-2-3-3 (a) and its corresponding equivalent gold nanoparticle tetrahedron (b). (c) Geometrical distances in a tetrahedral template. (d) Histogram of the estimated edge length D over 205 projected tetramers and its Gaussian distribution (16 ± 2.5 nm).

For the isomer 1-1-2-3-3, we reconstructed a theoretical tetrahedron that matches best the 225 imaged tetramers. To do so, we first measured the six interparticle distances l_1 to l_6 for the 225 tetramers (Supplementary Fig. S18a). A tetrahedron can be defined by three variables: D, the edge length of an equivalent DNA template, and the two rotation angles around the x-axis and the y-axis, θ_x and θ_y (Supplementary Fig. S18b). From D, it is possible to determine the centre-to-centre distance S (Supplementary Fig. S18c) with the following trigonometric formula: $S = D + \sqrt{8/3} * (T + d/2)$, with T the length of the four thymine hinge and the trithiol linker ($T \approx 2$ nm) and d the diameter of the gold nanoparticle (Supplementary Fig. S16c). By projecting the six centre-to-centre segments S on the xy-plan, we obtain a set of 6 interparticle distances $l'_i(D, \theta_x, \theta_y)$. We determined the best fitting tetrahedron by minimising the sum $R(D, \theta_x, \theta_y) = \sum_{i=1}^{6} \sqrt{(l_i - l'_i(D, \theta_x, \theta_y))^2}$. The average edge length of the theoretical tetrahedron is $D = 16 \pm 2.5$ nm which is 6 nm longer than

a theoretically fully extended DNA tetrahedron (10.2 nm). This demonstrates that the synthesised tetramers are not tetrahedra.

Optical properties

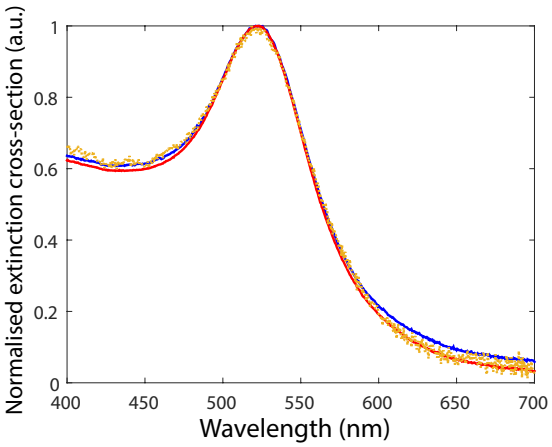

Figure S19: Normalised extinction spectra of monomers (blue line), dimers (red line - structure 14) and tetramers (orange line - isomer 1-1-2-3-3)

The Supplementary Fig. S19 shows that the extinction cross-sections of dimers and tetramers with the shortest interparticle distances overlay with the cross-section of single particles. It demonstrates that the ratios between the interparticle distances and particle size is beyond coupling limits.